Kinetic Energy Distribution of H($2p$) Atoms from Dissociative Excitation of H_2

Joseph M. Ajello, Syed M. Ahmed, Isik Kanik, and Rosalie Multari
Jet Propulsion Laboratory, California Institute of Technology, Pasadena, California 91109
(Received 2 February 1995)

The kinetic energy distribution of H($2p$) atoms resulting from electron impact dissociation of H_2 has been measured for the first time with uv spectroscopy. A high resolution uv spectrometer was used for the measurement of the H Lyman-α emission line profiles at 20 and 100 eV electron impact energies. Analysis of the deconvolved 100 eV line profile reveals the existence of a narrow line peak and a broad pedestal base. Slow H($2p$) atoms with peak energy near 80 meV produce the peak profile, which is nearly independent of impact energy. The wings of H Lyman-α arise from dissociative excitation of a series of doubly excited Q_1 and Q_2 states, which define the core orbitals. The fast atom energy distribution peaks at 4 eV.

PACS numbers: 34.80.Ht, 33.50.Dq

The kinetic distribution of H($2s$) atoms from dissociative excitation of H_2 has been the subject of much published research [1–7], particularly in the late 1960s through 1980. The kinetic energy distribution function of H($2p$) atoms from dissociative excitation of H_2 has not previously been measured. The cross section for this process is the largest of H_2 dissociative excitation processes [8], and a study of this process is paramount for an understanding of dissociation of H_2. There are expected to be two distinct maxima in the H($2p$) kinetic energy distribution by analogy to results obtained from the distribution of H($2s$) and H(nl) atoms, where $n = 3, 4$, and 5. A comparison of the H($2p$) and H($2s$) distributions is of fundamental importance in understanding the dynamics of the H_2 dissociation process which can occur from singly excited or doubly excited states. The former lead to the "slow" component and the latter lead to the "fast" component. In the separated atom limit, nonadiabatic coupling of the nearly degenerate $2p$ and $2s$ states is expected to lead to crossover of the H($2p$) and H($2s$) fragments [9]. For higher principal quantum numbers through $n = 5$, studies of H(nl) kinetic energy distribution function have been carried out for many years by Ogawa and co-workers [10–13]. Their interferometric technique involves measurement of the Doppler line profile of Balmer-α, -β, and -γ in the visible and near uv portion of the spectrum. The Balmer-α line profile, for example, shows a characteristic narrow central peak (~300 mÅ FWHM) and a broad wing (~1.8 Å FWHM). However, the Balmer-α line profile is three separate multiplets from H($3s, 3p, 3d$) excited states. Balmer-α has not been measured with sufficient resolution to study the slow atom distribution. In this work a spectroscopic technique was employed using a 3-m high resolution vacuum ultraviolet (vuv) spectrometer. Since the Doppler wavelength shift is proportional to the emission line wavelength, 5 to 6 times narrower line profiles can be expected in the vuv, necessitating the use of fast Fourier transform (FFT) techniques to deconvolve line profiles. The H Lyman-α (L_α) multiplet structure is simple enough to yield both the slow and fast atom distributions from the deconvolved line profile.

Most measurements of H($2s$) kinetic energy distributions have been obtained by time-of-flight (TOF) techniques. The TOF spectra are complicated, in many cases, by the blending of signals from H($2s$) metastable atoms and high Rydberg atoms. The threshold appearance potentials (AP) are frequently uncertain to ± 1 eV or more. Great disparity exists with regard to the threshold for the fast H($2s$) component compared to that of higher members of the Rydberg series. Misakian and Zorn [1] identified an AP at 29 eV for $n = 2$. Spezeski, Kalman, and McIntyre [4] pointed out that the AP must be less than 27 eV, whereas Ogawa and Higo [10] measured thresholds of 24 and 27 ± 1 eV for $n = 4$. In this work, we clearly identify three separate AP to ± 0.5 eV accuracy for the fast H($2p$) atoms.

Misakian and Zorn [1] placed the AP for slow H($2s$) atoms at 14.9 $\pm$ 0.3 eV. Direct dissociation and predissociation as well as resonance and cascade processes can contribute to this threshold for H($2s$) and H($2p$). We have recently modeled the total absolute emission cross section of H L_α into six separate fast and slow processes from low resolution studies of the unresolved H L_α line [8]. This work produces a direct measurement of the fraction of fast atoms and supports our method of analysis of total emission cross sections.

The experimental system has been described in a recent paper [14]. In brief, it consists of a high resolution 3-m uv spectrometer in tandem with an electron impact collision chamber. A resolving power of 50 000 is achieved by operating the spectrometer in third order. The line shapes were measured with experimental conditions that ensure linearity of signal with electron beam current and gas pressure. All spectral and cross section data were obtained in the crossed beams mode. The electron impact induced fluorescent line profiles of H L_α at 20 and 100 eV impact energies are shown in Fig. 1, along with the instrument slit function. As expected, the line profiles consist of a nar-

0031-9007/95/75(18)/3261(4)$06.00

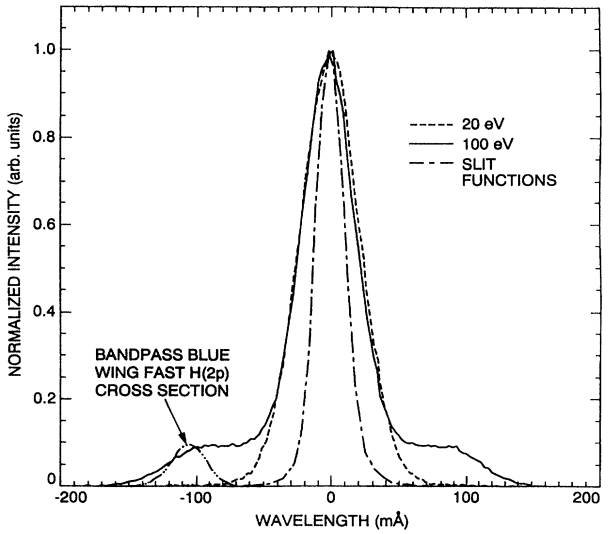

FIG. 1. Overplot of 20 and 100 eV H L_α line profile compared to the instrument slit function. The line profiles were measured in third order and the slit function was measured at zero order. The operating conditions were established as follows: (1) background gas pressure of 1×10^{-4} torr and (2) electron beam current of 269 μA. The data statistics were better than 1%. The wavelength step size was 2.667 mÅ. The FWHM of the H L_α features at 100 and 20 eV and the instrument slit function are 47, 49, and 24 mÅ, respectively. The placement of the instrument bandpass for the excitation function measurement of Fig. 4 is shown.

row central peak and a broad wing base at 100 eV impact energy. The line profile at 20 eV shows no pedestal base structure. It is perfectly symmetric. The line profiles were measured at 90° to the electron beam axis and molecular beam axis. The H L_α line is actually a closely spaced multiplet of doublet structure. The ^2P-^2S multiplet may be weakly polarized depending on the magnetic sublevel population and/or the spatial distribution of dissociation products [15]. We have acquired a vuv polarizer to complete this aspect of the study. In this study we assume the anisotropy is small. There is a small asymmetry (less than 6%) in the pedestal half-widths with respect to line center at 100 eV. Strong evidence for the near symmetry of the H L_α central peak comes from the measurement of the isotropy of the angular distribution of slow H(2s) atoms at threshold [1]. Above threshold the slow distribution is found to remain nearly isotropic in space since (1) many parallel and perpendicular transition matrix elements contribute to the slow atom (pre)dissociation process and (2) predissociation is a slow process compared to period of molecular rotation [1]. Similarly, our excitation function measurements will show that many parallel and perpendicular transitions contribute to the fast atom H(2p) distribution. Undoubtedly, a small angular anisotropy remains for fast H(2p) atoms above 30 eV impact energy from the importance of the $^1\Pi_u$ intermediate excited state [1].

The measured FWHM of 47 and 49 mÅ for the 100 and 20 eV line profiles, respectively, are not narrow with respect to the instrumental slit function (FWHM = 24 mÅ). FFT techniques were used to recover the actual line profile [16]. The measured line profile is the convolution of the true line profile and the instrumental slit function. The measured line profile $I(\lambda)$ is given by the following convolution integral:

$$I(\lambda) = \int T(\lambda')A(\lambda - \lambda')\,d\lambda', \qquad (1)$$

where $T(\lambda')$ is the true line profile at wavelength λ' and $A(\lambda - \lambda')$ is the instrumental response function.

The kinetic energy distribution of the fragments, $P(E)$, is given by

$$P(E) = k\,dT/d(\lambda), \qquad (2)$$

where k is a multiplicative constant [10]. The kinetic energy distribution of the H(2p) fragments is shown in Fig. 2 for the slow fragment distribution and in Fig. 3 for the combined fast and slow fragment H(2p) distributions. The kinetic energy distribution is obtained by finding the true line shape of H L_α from the FFT of Eq. (1). The deconvolved line profile of the central peak is found to have a FWHM of 40 ± 4 mÅ for both the 20 and 100 eV H L_α line profiles. Figure 2 shows the slow fragment H(2p) kinetic energy distribution for both the 100 and 20 eV line profiles given in Fig. 1. Since the measured H L_α line profile for the central peak at 100 eV is nearly identical to the 20 eV line profile, it follows that the resultant slow fragment distribution for each impact energy displays the same shape. The slow fragment energy distribution has a peak at 80 ± 10 meV and a FWHM of 260 ± 20 meV for both 20 and 100 eV impact energies. The results are compared to the H(2s) results of Misakian and Zorn [1].

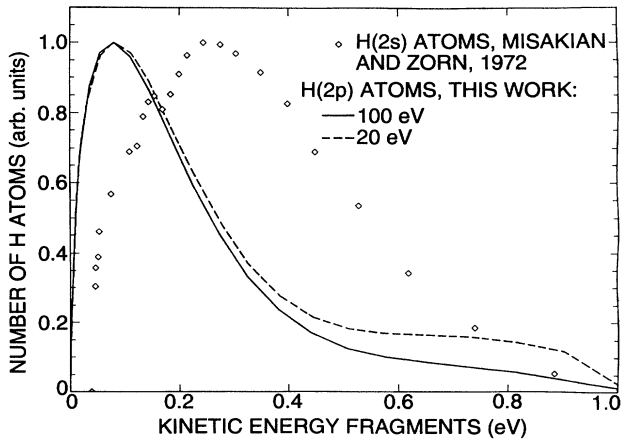

FIG. 2. Kinetic energy H(2p) distribution of slow atoms at both 20 and 100 eV compared to work of Misakian and Zorn [1].

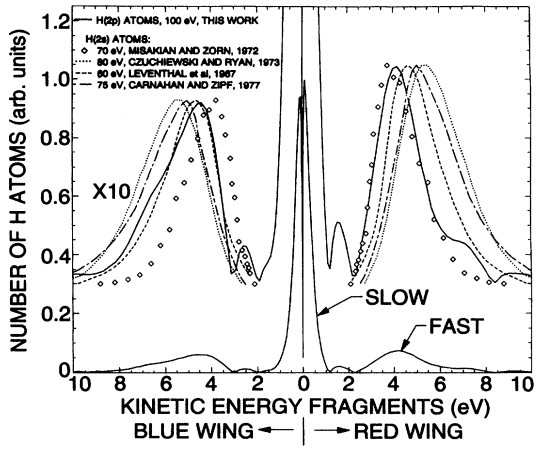

FIG. 3. Combined slow and fast H($2p$) atom distribution function compared to published results for fast H($2s$) atoms.

The combined slow and fast fragment energy distribution at 100 eV impact energy is shown in Fig. 3 for both the red and blue wings. The red wing is slightly more intense as shown in Fig. 1. The small difference in the energy distribution of the fast fragment distribution shape results from asymmetries in the pedestal line width in Fig. 1. Three peaks are observed in the distribution to be associated with either the blue or red wing. The strongest peak, near 80 meV and described above, arises from the slow atom distribution. The principal fast energy peak occurs at 4 ± 0.5 eV. The minor secondary fast energy peak occurs at about 2 ± 0.5 eV. The fast peak distribution is compared to H($2s$) results from four sets of authors. The experimental energies differ for the authors. All observations were at 90° with respect to the incident electron except for those of Misakian and Zorn [1] at 80° with respect to the electron beam axis. The results of Spezeski, Kalman, and McIntyre [4] (at 98 eV) are not shown on the plot but are nearly identical to those of Czuchlewski and Ryan [6] (at 80 eV). Our results for H($2p$) (at 100 eV) lie between the work of Misakian and Zorn [1] (at 70 eV) and Leventhal, Robiscoe, and Lea [7] (at 60 eV) and indicate that the fast $2s$ and $2p$ atoms come from the same channels. A resolution of the fast beam H($2s$) peak into two definite peaks at 4.4 ± 0.9 and 2.3 ± 0.5 eV has been reported only by Leventhal, Robiscoe, and Lea [7] at an angle of 77° with respect to the electron beam axis. This result has been disputed by the data of Spezeski, Kalman, and McIntyre [4] who pointed out that Misakian and Zorn [1] did not find this double peak in their data. In addition, they pointed out the outstanding problem for the fast peak(s) which is: What other dissociating channels beside $Q_2(^1\Pi_u)$ autoionizing states that dissociate into H($2p, 2s, 1s$) + H($2p, 2s$) contributed to this distribution? They concluded that other states contribute, and their main evidence was a model of the changing energy dependence of the H($2s$) distribution function with electron impact energy. However, accurate experimental excitation function studies were needed.

We measured the accurate function for the fast atom component. By placing the center of the bandpass of the spectrometer on the blue wing at 104 mÅ from the line center and restricting the FWHM of the bandpass to 36 mÅ, we were able to obtain a data set that clearly shows the threshold for the fast processes. The base of the red edge of the bandpass extended to within 70 mÅ of the central peak and for this reason the bandpass captures a very small portion of the wing of the central peak. This overlap is demonstrated in Fig. 1. The excitation function for the blue wing is shown in Fig. 4. The first threshold is at 16.7 ± 0.5 eV and corresponds to pairs of slow atoms from the central peak with total kinetic energy of near 2 eV. As explained above, blue light leak from the base of the central peak accounts for this threshold. Above 16.67 eV, cascade from H_α contributes to the central peak line profile. However, at this threshold energy the kinetic energy of H($2p$) atoms from cascade is zero. The small signal from the slow atom distribution can be considered as background to the fast atom signal. The other three thresholds can be traced to doubly excited states of H_2 which have the lowest $^2\Sigma_u^+$ and first excited $^2\Pi_u$ states of H_2^+ as core orbitals. They are designated Q_1 and Q_2, respectively [17]. Fundamental calculations by Guberman [17] allowed us to identify where the Q_1 and Q_2 states cross the right-hand edge of the Franck-Condon region. The most closely aligned thresholds of Guberman are associated with the measurement. In some cases more than one threshold lies within 0.5 eV of the measurement uncertainty. For the first time, dissociation along the $n = 2$ asymptote is clearly identified as arising from a doubly excited state of H_2 at the lowest threshold of 23.0 eV. According to Guberman the Q_1 $[^1\Sigma_g^+(1)]$ state is the responsible intermediate state. This same threshold has been found in

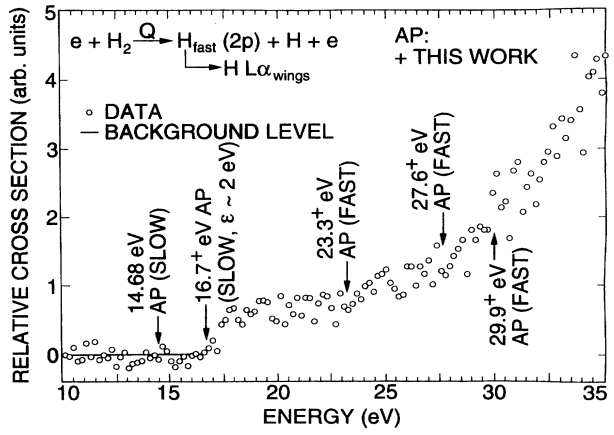

FIG. 4. Optical excitation function of H L_α line blue wing. The channel spacing is 200 meV. The electron gun energy resolution is 300 meV. The energy scale was calibrated from the 14.68 eV AP of the line center.

other electron impact experiments: (1) dissociative excitation leading to $n = 4$ product detected by Balmer-β radiation [10], (2) dissociative excitation producing high Rydberg atoms studied by TOF techniques [18], and (3) dissociative ionization processes producing H^+ ions measured by an ion mass spectrometer [19]. In all cases mentioned, perturbations from homogeneous interactions between the Q_1 $[^1\Sigma_g^+(1)]$ state and the dissociating (e.g., $E, F\ ^1\Sigma_g^+$ state for our case for $n = 2$) or autoionizing state has led to the same threshold. Nonadiabatic coupling of the first five $^1\Sigma_g^+$ states of H_2 has been recently treated on an *ab initio* basis by Wolniewicz and Dressler [20].

The next threshold is at 27.6 eV and can arise from the Q_1 $[^1\Sigma_g^+(2)]$ state at 27.2 eV, Q_1 $[^{3,1}\Pi_g(2)]$ states at 27.4 and 27.5 eV, respectively, Q_1 $[^{3,1}\Pi_u(2)]$ states at 27.5 and 27.6 eV, respectively and/or Q_1 $[^1\Sigma_u^+(2)]$ at 27.8 eV. However, the selection rules for molecular dissociation at threshold, arising from excitation from the $^1\Sigma_g^+$ ground state and viewed 90° to the electron beam axis, do not allow any Π_g or $^1\Sigma_u^+$ intermediate repulsive states [21]. In the center of the Franck-Condon region the kinetic energy released by the allowed transitions to the repulsive Q_1 states amounts to approximately 6.5 eV or more per $H(2p)$ atom and contributes to the bump in the kinetic energy distribution between 6 and 8 eV in Fig. 3. The final sharp threshold in Fig. 4 at 29.9 eV correlates with a set of Q_2 $(^1\Sigma_g^+, ^{1,3}\Pi_u)$ states between 30 and 32 eV. Thus many dissociation channels contribute to the fast atom dissociation process as predicted by Spezeski, Kalman, and McIntyre [4]. The steep rise in cross section beginning at 30 eV and the kinetic energy distribution energy dependence for fast fragments at 100 eV verifies that the dominant contribution to the fast $H(2p)$ distribution arises from Q_2 $(^1\Sigma_g^+, ^1\Pi_u)$ states as previously concluded for $H(2s)$ [1,4].

In conclusion, many new results can be gleaned from the H L_α line profile measurement and the derived $H(2p)$ kinetic energy distribution. Our earlier result described the H L_α dissociation cross-section budget at 100 eV [13]. In brief, the low resolution cross-section budget predicted that the partitioning of dissociation from singly excited states (slow atoms) and doubly excited states (fast atoms) occurred with a fractional percentage of 0.73 and 0.27, respectively. Integrating under the kinetic energy distribution in Fig. 4 gives a fractional percentage of 0.69 and 0.31, respectively. This verification testifies to the usefulness of the modified Born equation developed by this laboratory [22]. The modified Born equation gives the absolute cross sections for each process. This slow/fast atom quantum yield at 100 eV is quite different than that found for $H(2s)$ by Carnahan and Zipf [3]. Their fractional percentage is 0.87 and 0.13, respectively.

The kinetic energy distribution of the fast $H(2s)$ and $H(2p)$ atoms appears to be identical from 2 to 10 eV. The slow atom $H(2p)$ distribution is different than the $H(2s)$ slow atom distribution. Cascade from the higher Rydberg states contributes to approximately 6% of the slow atom $H(2p)$ signal at 100 eV. $H(2s)$ contains less than 1% contribution from cascade at this energy [16]. Both distributions are shown in Fig. 3 and have a high energy cutoff near 1 eV. Ryan *et al.* [5] pointed out that TOF techniques lose sensitivity as the energy approaches zero. Based upon this, the difference is significant. uv techniques do not have a sensitivity problem at low energy.

This work was supported by the Air Force Office of Scientific Research (AFOSR), the Aeronomy Program of the National Science Foundation Program (Grant No. ATM-9320589), and NASA Planetary Atmospheres, Astronomy/Astrophysics and Space Physics Program Offices. S. Ahmed and R. Multari were each supported by a National Research Council Resident Research Associateship.

[1] M. Misakian and J. C. Zorn, Phys. Rev. A **6**, 2180 (1972).
[2] R. Clampitt, Phys. Lett. **28A**, 581 (1969).
[3] B. L. Carnahan and E. C. Zipf, Phys. Rev. A **16**, 991 (1977).
[4] J. J. Spezeski, O. F. Kalman, and L. C. McIntyre, Phys. Rev. A **22**, 1906 (1980).
[5] S. R. Ryan, J. J. Spezeski, O. F. Kalman, W. E. Lamb, L. C. McIntyre, and W. H. Wing, Phys. Rev. A **19**, 2192 (1979).
[6] S. J. Czuchlewski and S. R. Ryan, Bull. Am. Phys. Soc. **18**, 688 (1973).
[7] M. Leventhal, R. T. Robiscoe, and K. R. Lea, Phys. Rev. **158**, 49 (1967).
[8] J. M. Ajello, D. E. Shemansky, and G. K. James, Astrophys. J. **371**, 422 (1991).
[9] J. A. Beswick and M. Glass-Maujean, Phys. Rev. A **35**, 3339 (1987).
[10] T. Ogawa and M. Higo, Chem. Phys. Lett. **65**, 610 (1979).
[11] T. Ogawa and M. Higo, Chem. Phys. **52**, 55 (1980).
[12] K. Nakashima, M. Tanguchi, and T. Ogawa, Chem. Phys. Lett. **197**, 72 (1992).
[13] T. Ogawa, S. Ihara, and K. Nakahima, Chem. Phys. **161**, 509 (1992).
[14] X. Liu, S. M. Ahmed, R. Multari, G. K. James, and J. M. Ajello, "High Resolution Electron Impact Study of the FUV Spectrum of Molecular Hydrogen," Astrophys. J. Supp. (to be published).
[15] R. J. Van Brunt and R. N. Zare, J. Chem. Phys. **48**, 4304 (1968).
[16] W. H. Press, B. P. Flannery, S. A. Teukolsky, and W. T. Vettering, *Numerical Recipes* (Cambridge University Press, Cambridge, England, 1987).
[17] S. L. Guberman, J. Chem. Phys. **78**, 1404 (1983).
[18] J. A. Schiavone, K. C. Smyth, and R. S. Freund, J. Chem. Phys. **63**, 1043 (1975).
[19] A. Crowe and J. W. McConkey, Phys. Rev. Lett. **31**, 192 (1973).
[20] L. Wolniewicz and K. Dressler, J. Chem. Phys. **100**, 444 (1994).
[21] G. H. Dunn, Phys. Rev. Lett. **8**, 62 (1962).
[22] D. E. Shemansky, J. M. Ajello, D. T. Hall, and B. Franklin, Astrophys. J. **296**, 774 (1985).